GDCh Research Article Angewandte International Edition Chemie www.angewandte.org

How to cite: Angew. Chem. Int. Ed. 2024, e202405451
doi.org/10.1002/anie.202405451

VIP HOFs Very Important Paper

Modulating the Microenvironments of Robust Metal Hydrogen-Bonded Organic Frameworks for Boosting Photocatalytic Hydrogen Evolution

Chong-Jiu Lu[+], Wen-Jie Shi[+], Yun-Nan Gong, Ji-Hong Zhang, Yu-Chen Wang, Jian-Hua Mei, Zhao-Ming Ge, Tong-Bu Lu, and Di-Chang Zhong**

Abstract: Hydrogen-bonded organic frameworks (HOFs) are outstanding candidates for photocatalytic hydrogen evolution. However, most of reported HOFs suffer from poor stability and photocatalytic activity in the absence of Pt cocatalyst. Herein, a series of metal HOFs (Co_2-HOF-X, X=COOMe, Br, tBu and OMe) have been rationally constructed based on dinuclear cobalt complexes, which exhibit exceptional stability in the presence of strong acid (12 M HCl) and strong base (5 M NaOH) for at least 10 days. More impressively, by varying the -X groups of the dinuclear cobalt complexes, the microenvironment of Co_2-HOF-X can be modulated, giving rise to obviously different photocatalytic H_2 production rates, following the –X group sequence of –COOMe > –Br > –tBu > –OMe. The optimized Co_2-HOF-COOMe shows H_2 generation rate up to 12.8 mmol g^{-1} h^{-1} in the absence of any additional noble-metal photosensitizers and cocatalysts, which is superior to most reported Pt-assisted photocatalytic systems. Experiments and theoretical calculations reveal that the –X groups grafted on Co_2-HOF-X possess different electron-withdrawing ability, thus regulating the electronic structures of Co catalytic centres and proton activation barrier for H_2 production, and leading to the distinctly different photocatalytic activity.

Introduction

The increasing combustion of fossil fuels has caused serious energy and environmental issues.[1] Sunlight-driven water splitting to clean hydrogen has been recognized as one of the most promising approaches to solve these problems.[2] Over the past several decades, a variety of porous crystalline materials such as metal–organic frameworks (MOFs), covalent organic frameworks (COFs) and hydrogen-bonded organic frameworks (HOFs) have been developed to catalyze this important reaction because of their well-defined and tailorable structures, as well as high surface area and semiconductor-like behavior.[3] Amongst them, HOFs assembled by organic or metal–organic building blocks through hydrogen-bonding interactions, which are often further strengthened via π–π stacking or van der Waals forces, have attracted more and more attention in photocatalysis due to their unique features of mild synthetic conditions, easy healing and regeneration.[4] Nevertheless, compared with MOFs and COFs constructed by coordination bonds and covalent bonds respectively, the hydrogen-bonding interactions within HOFs are weaker, which usually lead to the decomposition of HOF frameworks during the photocatalytic process.[5] Therefore, the development of robust HOFs for photocatalytic H_2 production is highly desirable yet remains challenging.

In addition to the low stability, most of HOFs also suffer from unsatisfactory photocatalytic performance for H_2 production due to the fast recombination of photogenerated electron and hole.[4g–j] To conquer this, the introduction of noble-metal cocatalysts (e.g. Pt) into the catalytic system has been proven facile and effective.[4g–k] However, the high cost and shortage of noble metals impede their large-scale practical applications. Hence, it is crucial to construct non-noble metal yet high-performance HOF photocatalysts. Recently, some other strategies have been developed to promote the charge separation in photocatalysts, among them, the microenvironment modulation, inspired by natural enzyme catalysis that can obviously improve catalytic activity, selectivity and stability, has been regarded as the most direct and effective method.[6] This is due to the spatial structures and electronic properties around catalytic sites can be dramatically changed after microenvironment modulation, thus leading to distinctly different catalytic behavior.[7] In particular, the introduction of electron-withdrawing or electron-donating groups around the catalytic sites has been considered as an outstanding approach to realize microenvironment modulation.[8] Considering the characteristics of HOFs, they would be the ideal models to achieve in-depth insights into the significant roles of microenvironment modulation in photocatalysis. However, related research has not been documented up to now, to the best of our knowledge.

[*] C.-J. Lu,[+] Dr. W.-J. Shi,[+] Dr. Y.-N. Gong, J.-H. Zhang, Y.-C. Wang, J.-H. Mei, Z.-M. Ge, Prof. Dr. T.-B. Lu, Prof. Dr. D.-C. Zhong
Institute for New Energy Materials and Low Carbon Technologies, School of Materials Science and Engineering, Tianjin University of Technology, Tianjin 300384, China
E-mail: yngong@email.tjut.edu.cn
dczhong@email.tjut.edu.cn

[+] These authors contributed equally

In this work, we successfully constructed four new metal HOFs (denoted by Co_2-HOF-X, X = COOMe, Br, tBu and OMe, X represents the changeable functional groups grafted onto the benzene rings in ligand) by connecting dinuclear cobalt complexes through hydrogen bonds for photocatalytic hydrogen evolution. These HOFs exhibit exceptionally high stability in extreme conditions of 12 M HCl and 5 M NaOH solutions for at least 10 days. Furthermore, the slightly alterable microenvironment of Co_2-HOF-X regulates the electronic state of Co catalytic centers and proton activation barrier for hydrogen evolution, as demonstrated by a series of experiments and theoretical calculations. As a result, the photocatalytic H_2 production rates of Co_2-HOF-X follow the -X group sequence of –COOMe > –Br > –tBu > –OMe, among which, the optimized Co_2-HOF-COOMe presents an excellent photocatalytic H_2 production rate of 12.8 mmol g^{-1} h^{-1} in absence of additional noble-metal photosensitizer and cocatalyst, which is higher than most of reported Pt-assisted photocatalytic systems. To our knowledge, this is the first report on regulating photocatalysis by microenvironment modulation in HOFs.

Results and Discussion

The (1*E*,3*E*)-2-hydroxyisophthalaldehyde dioxime derivatives (HID–X, X=COOMe, Br, tBu and OMe) ligands were first synthesized according to the literatures.[9] The results of ^{1}H nuclear magnetic resonance (NMR) spectra show that HID–X were successfully obtained with high purity (Figures S1–S4). Then, the dinuclear cobalt complexes (Co_2–X) with diverse functional groups grafted onto the benzene rings in ligands were prepared by the reaction of HID–X, 1-pyrenylboronic acid (PBA) and $Co(NO_3)_2 \cdot 6H_2O$ in a mixed solution of methanol and ethanol at 70 °C for 20 min (Figure 1). Fourier transform infrared spectroscopy (FTIR) spectra of these complexes exhibit the absence of the hydroxyl stretching vibration band at about 3274 cm^{-1} compared with both HID–X and PBA (Figures S5–S8). Liquid chromatography mass spectrometry (LC–MS) of these complexes show the ion peaks at *m/z* 1247.1394, 1308.8593, 1241.3126 and 1163.1561, corresponding to the species of $[Co_2–COOMe]^-$, $[Co_2–Br]^-$, $[Co_2–tBu]^-$ and $[Co_2–OMe]^-$, respectively (Figures S9–S12). These results suggest that the dinuclear cobalt complexes with different functional groups were successfully prepared. Subsequently, the dinuclear cobalt complexes were dissolved in *N*,*N*-dimethylformamide (DMF), followed by slowly diffusing ethanol or isopropanol and H_2O, which were kept at 18 °C for 10 days to yield orange block-shaped crystals of Co_2-HOF-X. Single-crystal X-ray diffraction unveils that Co_2-HOF-COOMe, Co_2-HOF-Br and Co_2-HOF-OMe crystallize in the monoclinic system with the I_2/a, $P2_1/c$ and Cc space groups, and Co_2-HOF-tBu crystallizes in the orthorhombic system and Fdd_2 space group (Table S1). As shown in Figures 1 and S13–S16, the Co ions in Co_2-HOF-X exhibit the same coordination geometry, with each Co six-coordinated by three hydroxyl oxygen and three imine nitrogen atoms. Two adjacent Co ions in each dinuclear cobalt complex were linked via sharing three hydroxyl oxygen atoms. In Co_2-HOF-X, the dinuclear cobalt complexes are connected through C–H··O and/or C–H··π hydrogen bonds to generate two-dimensional (2D) layers (Figures S17–S20, Table S2). Neighboring 2D layers are linked via C–H··O or C–H··π hydrogen bonds to form three-dimensional (3D) frameworks (Figure 1), which are further stabilized by π–π stacking interactions (Table S2). In addition, Co_2-HOF-X are anionic frameworks, which are balanced by tetraethylammonium cations (Figures S13–S16).

The experimental powder X-ray diffraction (XRD) patterns of Co_2-HOF-X are basically identical to the simulated ones, demonstrating their high phase purities (Figures S21–S24). The porosity of Co_2-HOF-X was first confirmed by CO_2 adsorption measurements. As shown in Figures 2a and S25, Co_2-HOF-COOMe, Co_2-HOF-Br, Co_2-HOF-tBu and Co_2-HOF-OMe can adsorb 51.73, 48.17, 56.27 and 37.16 cm^3 g^{-1} CO_2 at 196 K and 1 atm, corresponding to Brunauer–Emmett–Teller (BET) surface areas of 220, 197, 270 and 172 m^2 g^{-1}. Moreover, the I_2 adsorption experiments were conducted by soaking Co_2-HOF-X in the *n*-hexane solution of I_2 to further examine their porosity. The adsorption of Co_2-HOF-X to I_2 was clearly observed by the color change of solution from pink to colorless after 8 h (Figures 2b and S26–S28). Furthermore, the results of UV/Vis spectroscopy demonstrate that the intensity of I_2 characteristic adsorption peak at about 521 nm gradually decreases along with the increased soaking time, which were nearly disappeared after 8 h, suggesting the presence of porosity in Co_2-HOF-X (Figures 2b and S26–S28). The thermal and chemical stabilities of Co_2-HOF-X were also investigated. The results of thermogravimetric analysis (TGA) show that Co_2-HOF-X are stable up to 260 °C (Figures S29–S32). The chemical stability of Co_2-HOF-X was investigated by soaking Co_2-HOF-X in harsh acid-base solutions. As shown in Figures 2c, 2d, S33 and S34, Co_2-HOF-X can maintain their crystallinity in 12 M HCl and 5 M NaOH solutions for at least 10 days, suggesting their exceptional chemical stability. Such high stability of Co_2-HOF-X can be attributed to their hydrophobicity and/or the strong π–π interactions (Figure S35 and Table S2).[4a,10]

The Co oxidation state of Co_2-HOF-X was tested by X-ray photoelectron spectroscopy (XPS). As shown in Figures 3a and S36, the Co 2p XPS spectra of Co_2-HOF-X display Co $2p_{1/2}$ and Co $2p_{3/2}$ characteristic peaks with corresponding satellite peaks, indicating that the oxidation state of Co species in Co_2-HOF-X is +2.[11] It's worth noting that the binding energy of Co $2p_{3/2}$ shows shift by changing functional groups in Co_2-HOF-X, following a sequence of –COOMe > –Br > –tBu > –OMe, positively correlated with the electron-withdrawing ability of the –X functional group (Figure 3a). This demonstrates the modulated electronic structures of Co via slight modulation of the chemical structure in Co_2-HOF-X. The light absorbance of Co_2-HOF-X was investigated by solid UV/Vis spectra. The results show that all Co_2-HOF-X can absorb ultraviolet and visible light (Figure 3b). The band-gap energies (E_g) of Co_2-HOF-COOMe, Co_2-HOF-Br, Co_2-HOF-tBu and Co_2-HOF-OMe were estimated by the Kubelka–Munk (KM) method based on solid UV/Vis

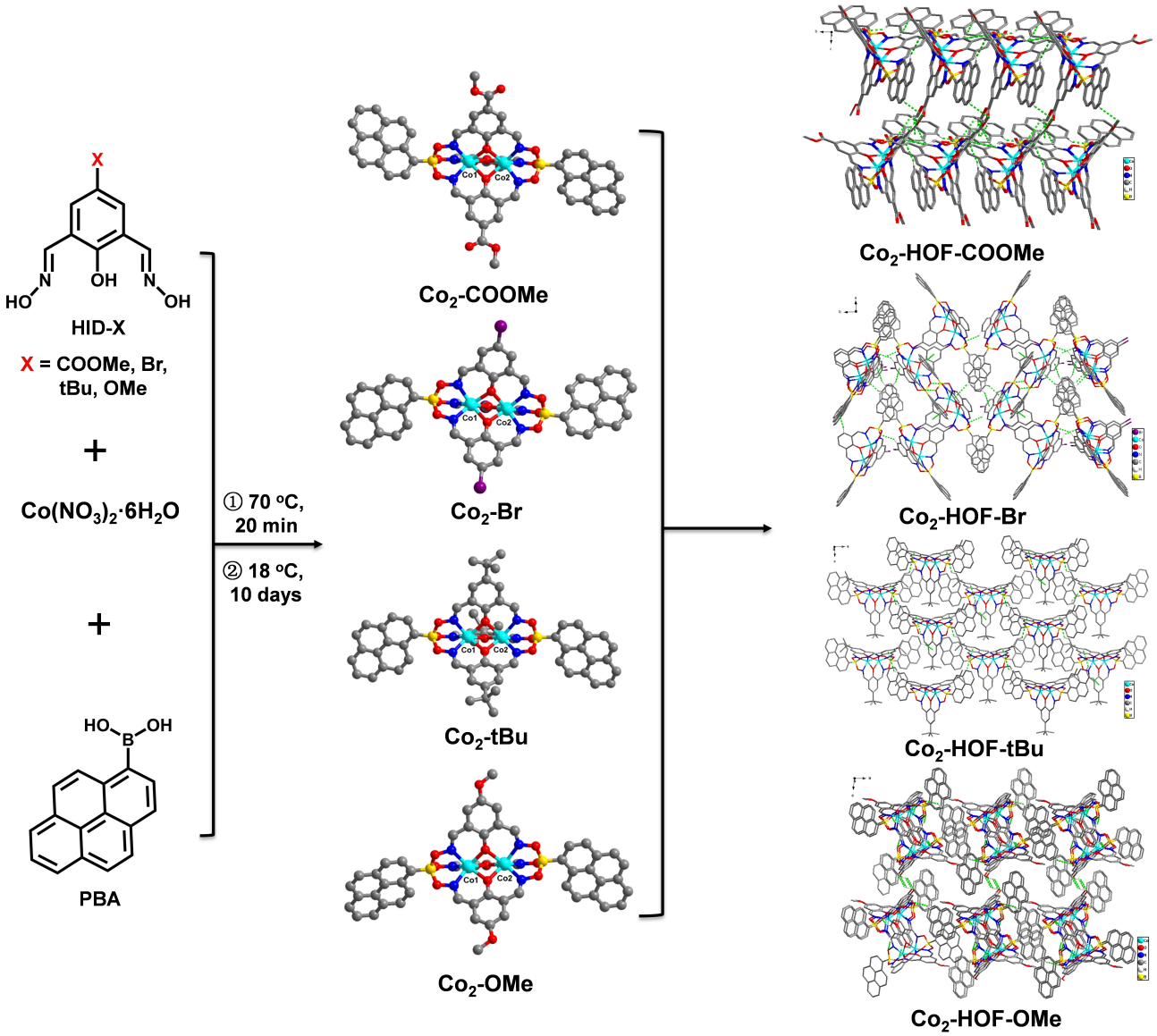

Figure 1. The syntheses and crystal structures of Co_2-HOF-X (X=COOMe, Br, tBu and OMe).

absorption spectroscopy, which are 2.08, 2.02, 2.09 and 1.73 eV, respectively (Figures S37–S40).[12] Furthermore, Mott–Schottky measurements of Co_2-HOF-X were carried out with the frequencies of 0.5, 1.0, and 1.5 kHz to determine their LUMO energy levels. All Co_2-HOF-X show the positive slopes of the C^{-2} values (vs. applied potentials), indicating that they are n-type semiconductors. The LUMO energy levels of Co_2-HOF-COOMe, Co_2-HOF-Br, Co_2-HOF-tBu and Co_2-HOF-OMe are determined by the intersection points of Mott–Schottky plots under different frequencies, which are −0.76, −0.51, −0.57 and −0.64 vs. NHE (Figures S41–S44), respectively.[13] Therefore, the HOMO energy levels of them are accordingly calculated to be 1.32, 1.51, 1.52 and 1.09 V vs. NHE, respectively (Figure S45). Note that all Co_2-HOF-X exhibit more negative LUMO energy levels than that of the proton reduction (0 V vs. NHE),[14] implying that these HOFs can theoretically achieve photocatalytic H_2 production.

In order to reveal how the different functional groups on Co_2-HOF-X affect the charge separation efficiency, a series of photo/electrochemical characterizations including photocurrent response, electrochemical impedance spectroscopy (EIS), photoluminescence (PL) emission and time-resolved PL (TRPL) spectra were carried out.[15] The results of photocurrent response demonstrate that the intensity follows an order of Co_2-HOF-COOMe > Co_2-HOF-Br > Co_2-HOF-tBu > Co_2-HOF-OMe, suggesting that Co_2-HOF-COOMe shows the fastest separation of photogenerated electron and hole (Figure 3c). This argument was supported by the EIS results, where the radius trend of Nyquist plots follows Co_2-HOF-COOMe < Co_2-HOF-Br < Co_2-HOF-tBu < Co_2-HOF-OMe, revealing the enhanced charge transfer resistance (Figure 3d). Moreover, the results of PL

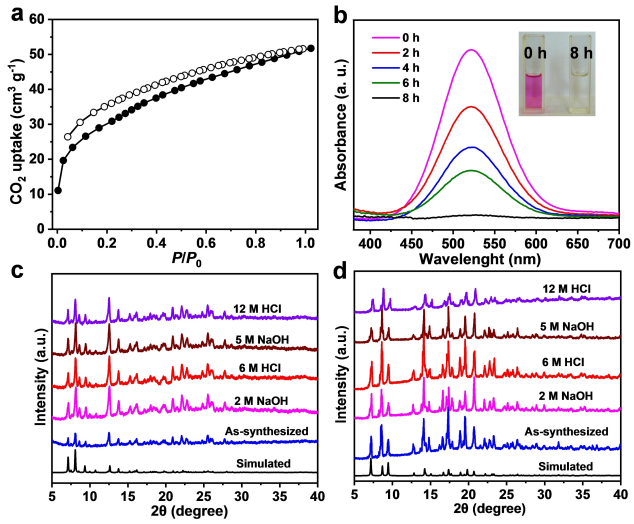

Figure 2. (a) CO_2 adsorption isotherm of Co_2-HOF-COOMe at 196 K. (b) UV/Vis spectra of I_2 *n*-hexane solution by soaking Co_2-HOF-COOMe at given intervals (Inset: photographic images of I_2 *n*-hexane solution at 0 and 8 h, respectively). Powder XRD patterns of Co_2-HOF-COOMe (c) and Co_2-HOF-tBu (d) treated with harsh acid-base solutions for 10 days.

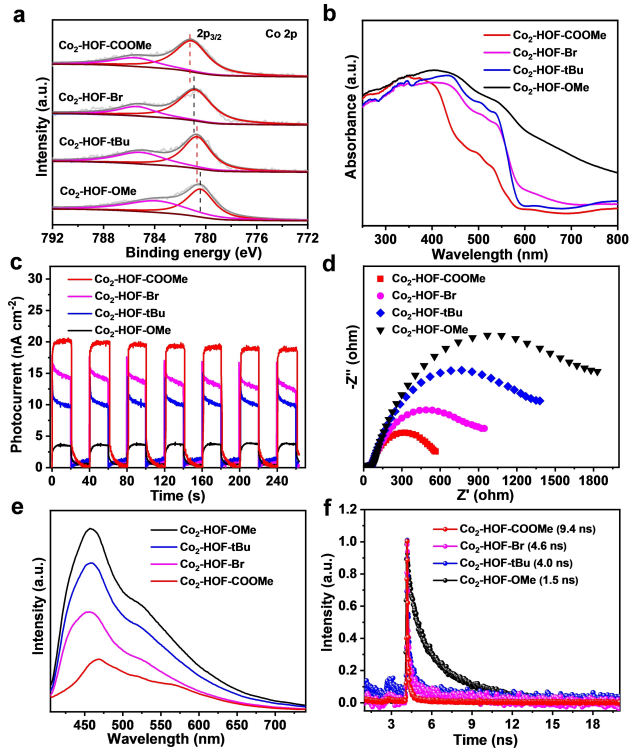

Figure 3. (a) Co $2p_{3/2}$ XPS spectra of Co_2-HOF-X. (b) UV/Vis spectra of Co_2-HOF-X. (c) Photocurrent response of Co_2-HOF-X. (d) EIS spectra of Co_2-HOF-X. (e) PL spectra of Co_2-HOF-X. (f) Transient fluorescence lifetime of Co_2-HOF-X.

spectra and TRPL show that the emission intensity is the weakest and PL average lifetime is the shortest for Co_2-HOF-COOMe among the four HOFs, further confirming the most efficient charge separation (Figure 3e and 3f). These results verify that the charge separation efficiency of Co_2-HOF-X follows a trend of Co_2-HOF-COOMe > Co_2-HOF-Br > Co_2-HOF-tBu > Co_2-HOF-OMe, suggesting that they might exhibit different catalytic activities and the Co_2-HOF-COOMe possesses the best activity in photocatalysis.

Encouraged by the results above, photocatalytic H_2 production over Co_2-HOF-X was investigated in CH_3CN/H_2O (v:v = 4:1) with 1,3-dimethyl-2-phenylbenzimidazoline (BIH) and triethylamine (TEA) as sacrificial electron donors and in absence of additional noble-metal photosensitizer and cocatalyst. As expected, the Co_2-HOF-X photocatalysts with only variation in the -X groups on the benzene rings of dinuclear cobalt complexes, exhibit notably different photocatalytic activities. As shown in Figure 4a and 4b, the H_2 production rates of Co_2-HOF-COOMe, Co_2-HOF-Br, Co_2-HOF-tBu and Co_2-HOF-OMe are 12.8, 10.7, 8.4 and 5.1 mmol g^{-1} h^{-1}, respectively. Among which, Co_2-HOF-COOMe achieves the highest H_2 generation rate, far surpassing most of reported Pt-assisted photocatalytic systems (Table S3). These results unambiguously highlight that the microenvironment modulation by Co_2-HOF-X plays a critical role in regulating the photocatalytic performance. The stability of Co_2-HOF-X was examined after photocatalytic reaction. The results of powder XRD patterns show that their good crystallinity can be maintained, unveiling their excellent structural stability (Figures S46–S49). Moreover, the results of inductively coupled plasma mass spectrometry (ICP-MS) measurements demonstrate that very limited Co^{2+} was leached for Co_2-HOF-X in the solution during the photocatalysis (Table S4). The best-performing Co_2-HOF-COOMe shows no noticeable degradation for H_2 production rate during the four consecutive runs, indicating its high catalytic stability (Figure 4c). Additionally, the apparent quantum efficiencies (AQE) of Co_2-HOF-X were measured at 365, 395 and 450 nm. As shown in Figure 4d, Co_2-HOF-X also exhibit different AQE, follow-

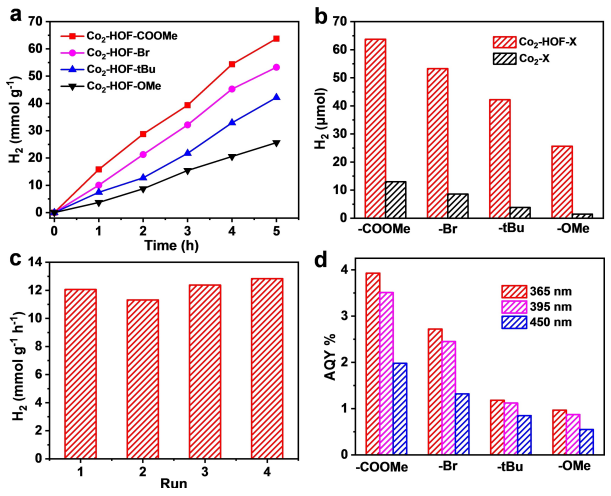

Figure 4. (a) Time-dependent photocatalytic H_2 evolution over Co_2-HOF-X. (b) Amounts of H_2 over Co_2-HOF-X and Co_2-X in 5 h. (c) The photocatalytic H_2 production rate of Co_2-HOF-COOMe in four consecutive runs (4 hours for each run). (d) The AQE values of Co_2-HOF-X.

ing the –X group sequence of –COOMe > –Br > –tBu > –OMe, in which the AQE of Co_2-HOF-COOMe reaches as high as 3.93 % at 365 nm.

To confirm the source of H_2, the photocatalytic experiment over Co_2-HOF-COOMe was performed in the absence of H_2O. Negligible H_2 was detected, unambiguously verifying that hydrogen source indeed comes from water splitting (Figure S50). Furthermore, the homogeneous photocatalytic experiments over Co_2-X (X=COOMe, Br, tBu and OMe) has also been evaluated in DMF/H_2O ($v:v=4:1$) with BIH and TEA as sacrificial electron donors. After 5 h of light irradiation, the H_2 yields of Co_2–COOMe, Co_2–Br, Co_2–tBu and Co_2–OMe are 12.97, 8.60, 3.81 and 1.46 μmol, respectively (Figure 4b). It' worth noting that the trend of catalytic activity for Co_2-HOF-X [Co_2-HOF-COOMe (63.8 μmol) > Co_2-HOF-Br (53.3 μmol) > Co_2-HOF-tBu (42.2 μmol) > Co_2-HOF-OMe (25.6 μmol) after 5 h of light irradiation] is the same as that of Co_2-X. These results demonstrate that the ordered heterogeneity of Co_2-X in Co_2-HOF-X only increase catalytic performance but do not change the activity trend. These observations indicate that the microenvironment modulation in Co_2-HOF-X by altering -X groups plays the major role in regulating photocatalytic H_2 evolution performance, despite the change of the crystal structures and build-in-field in Co_2-HOF-X may also have influence on the H_2 evolution performance. Additionally, the homogeneous photocatalytic experiment of HID-COOMe for H_2 evolution with Pt as the cocatalyst was conducted. The H_2 yield was only 2.37 μmol within 5 h (Figure S51), which is obviously smaller than those of Co_2-COOMe (8.60 μmol) and Co_2-HOF-COOMe (63.8 μmol), suggesting that the Co and pyrene can be used as excellent catalytic site and photosensitive group, respectively.

The possible mechanism in the photocatalytic process was further elucidated by in situ electron paramagnetic resonance (EPR) and XPS measurements. Taking Co_2-HOF-COOMe as a representative, the EPR spectrum of Co_2-HOF-COOMe in the dark shows a broad signal at g = 2.18, which can be assigned to the paramagnetic Co^{2+}.[16] Upon light irradiation, this signal weakens, suggesting that part of Co^{2+} was transformed to diamagnetic Co^{+} (Figure 5a). Moreover, the Co 2p XPS spectrum of Co_2-HOF-COOMe displays two characteristic peaks at 781.2 and 796.9 eV in the dark, corresponding to the binding energies of Co $2p_{3/2}$ and Co $2p_{1/2}$ respectively, which shift to 780.8 and 796.6 eV upon light illumination, implying that the Co^{2+} accepts the photogenerated electrons (Figure S52).[13a,17] These results suggest that the Co_2-HOF-COOMe harvests light to generate electrons and holes, where electrons shift to the Co centers to reduce Co^{2+} to Co^{+}. Owing to the Co_2-HOF-X can theoretically achieve photocatalytic H_2 production characterized by the results of Mott–Schottky plots. Thus, the H^+ can be easily reduced to H_2 by Co^{+}, as some reported Co-based catalysts.[18] Moreover, the photogenerated holes are annihilated by TEA and BIH sacrificial agents.

To understand the distinctly different photocatalytic activity in Co_2-HOF-X by microenvironment modulation, density functional theory (DFT) calculations were carried

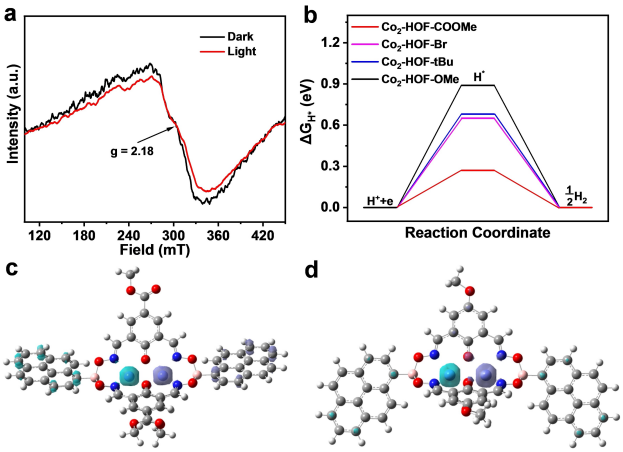

Figure 5. (a) EPR spectra of Co_2-HOF-COOMe in the dark and upon light irradiation. (b) The energy profiles of Co_2-HOF-X. Spin density maps of Co centers of Co_2-HOF-COOMe (c) and Co_2-HOF-OMe (d).

out by using Co_2-X complexes as calculation models based on the periodic structures of Co_2-HOF-X. As shown in Figure 5b, Co_2-HOF-X exhibit different ΔG_{H^*} (Gibbs free energy variation) with an order of Co_2-HOF-COOMe < Co_2-HOF-Br < Co_2-HOF-tBu < Co_2-HOF-OMe. Obviously, Co_2-HOF-COOMe shows the lowest ΔG_{H^*} of 0.27 eV, implying the most efficient proton/electron transfer to form H*, thus promoting the H_2 production. Moreover, the spin population of Co centers of Co_2-HOF-X was calculated to further elucidate their different photocatalytic activity (the larger population, the easier to give electrons).[10b] As shown in Figures 5c, 5d, S53 and Table S5, the population of Co centers in Co_2-HOF-X are different with an order of Co_2-HOF-COOMe > Co_2-HOF-Br > Co_2-HOF-tBu > Co_2-HOF-OMe. Among which, the Co centers of Co_2-HOF-COOMe has the highest population, demonstrating that it is the easiest to give electrons to combine with H^+ to form H*, thereby facilitating the H_2 production. These results agree well with the photocatalytic activity in experiments, manifesting again that the microenvironment modulation is an effective strategy to boost photocatalytic performance.

Conclusion

In summary, we have successfully fabricated four metal HOFs (Co_2-HOF-X, X=COOMe, Br, tBu and OMe) with outstanding chemical stability for photocatalytic hydrogen evolution. These HOFs not only retain structural integrity in strong acid solution (12 M HCl) but also in strong base solution (5 M NaOH). Moreover, the microenvironment of Co_2-HOF-X can be modulated by simply altering the -X group on the dinuclear cobalt complexes. As a result, Co_2-HOF-COOMe with the most electron-withdrawing group, exhibit the highest photocatalytic activity with H_2 generation rate of 12.8 mmol g^{-1} h^{-1}, in absence of additional noble-metal photosensitizer and cocatalyst, far surpassing the most of reported Pt-assisted photocatalytic systems. Systematic studies demonstrate that the significantly enhanced catalytic

performance of Co_2-HOF-COOMe can be attributed to the enhanced charge separation efficiency and lowered energy barrier of hydrogen-adsorption. This study provides a new way in developing HOF-based efficient photocatalysts for hydrogen evolution.

Acknowledgements

This work was supported by National Key R&D Program of China (2022YFA1502902), the National Natural Science Foundation of China (22371208, 22271218, 22071182, 22001043, 21931007).

Conflict of Interest

The authors declare no conflict of interest.

Data Availability Statement

The data that support the findings of this study are available in the supplementary material of this article.

Keywords: Hydrogen-bonded organic frameworks · dinuclear cobalt complexes · microenvironment modulation · photocatalysis · hydrogen evolution

[1] a) N. F. Suremann, B. D. McCarthy, W. Gschwind, A. Kumar, B. A. Johnson, L. Hammarström, S. Ott, *Chem. Rev.* **2023**, *123*, 6545–6611; b) D.-C. Zhong, Y.-N. Gong, C. Zhang, T.-B. Lu, *Chem. Soc. Rev.* **2023**, *52*, 3170–3214.

[2] a) Z.-Y. Shi, X. Zhang, X.-Q. Lin, G.-G. Liu, C.-Y. Ling, S.-B. Xi, B. Chen, Y.-Y. Ge, C.-L. Tan, Z.-C. Lai, Z.-Q. Huang, X.-Y. Ruan, L. Zhai, L.-J. Li, Z.-J. Li, X.-X. Wang, G.-H. Nam, J.-W. Liu, Q.-Y. He, Z.-Q. Guan, J.-L. Wang, C.-S. Lee, A. R. J. Kucernak, H. Zhang, *Nature* **2023**, *621*, 300–305; b) D. Voiry, H. S. Shin, K. P. Loh, M. Chhowalla, *Nat. Chem. Rev.* **2018**, *2*, 0105; c) W.-K. Qin, C.-H. Tung, L.-Z. Wu, *J. Mater. Chem. A* **2023**, *11*, 12521–12538; d) R. M. Bullock, J. G. Chen, L. Gagliardi, P. J. Chirik, O. K. Farha, C. H. Hendon, C. W. Jones, J. A. Keith, J. Klosin, S. D. Minteer, R. H. Morris, A. T. Radosevich, T. B. Rauchfuss, N. A. Strotman, A. Vojvodic, T. R. Ward, J. Y. Yang, Y. Surendranath, *Science* **2020**, *369*, 6505.

[3] a) C. Gropp, T.-Q. Ma, N. Hanikel, O. M. Yaghi, *Science* **2020**, *370*, 6515; b) Z.-E. Li, T. He, Y.-F. Gong, D.-L. Jiang, *Acc. Chem. Res.* **2020**, *53*, 1672–1685; c) D.-L. Jiang, *Chem* **2020**, *6*, 2461–2483; d) G.-R. Cai, P. Yan, L.-L. Zhang, H.-C. Zhou, H.-L. Jiang, *Chem. Rev.* **2021**, *121*, 12278–12326; e) Y. Liang, E. Li, K.-Y. Wang, Z.-J. Guan, H.-H. H. He, L.-L. Zhang, H.-C. Zhou, F.-H. Huang, Y. Fang, *Chem. Soc. Rev.* **2022**, *51*, 8378–8405; f) P.-H. Li, M. R. Ryder, J. F. Stoddart, *Acc. Mater. Res.* **2020**, *1*, 77–87.

[4] a) Q. Yin, P. Zhao, R.-J. Sa, G.-C. Chen, J. Lu, T.-F. Liu, R. Cao, *Angew. Chem. Int. Ed.* **2018**, *57*, 7691–7696; *Angew. Chem.* **2018**, *130*, 7817–7822; b) A.-A. Zhang, D.-H. Si, H.-B. Huang, L. Xie, Z.-B. Fang, T.-F. Liu, R. Cao, *Angew. Chem. Int. Ed.* **2022**, *61*, e202203955; *Angew. Chem.* **2022**, *134*, e202203955; c) Y.-S. Yang, L.-B. Li, R.-B. Lin, Y.-X. Ye, Z.-Z. Yao, L. Yang, F.-H. Xiang, S.-M. Chen, Z.-J. Zhang, S.-C. Xiang, B.-L. Chen, *Nat. Chem.* **2021**, *13*, 933–939; d) X.-Y. Song, Y. Wang, C. Wang, X.-Y. Gao, Y.-M. Zhou, B.-L. Chen, P. Li, *J. Am. Chem. Soc.* **2024**, *146*, 627–634; e) Y.-B. He, S.-C. Xiang, B.-L. Chen, *J. Am. Chem. Soc.* **2011**, *133*, 14570–14573; f) B. Han, H.-L. Wang, C.-M. Wang, H. Wu, W. Zhou, B.-L. Chen, J.-Z. Jiang, *J. Am. Chem. Soc.* **2019**, *141*, 8737–8740; g) N. Zhang, Q. Yin, S. Guo, K.-K. Chen, T.-F. Liu, P. Wang, Z.-M. Zhang, T.-B. Lu, *Appl. Catal. B* **2021**, *296*, 120337; h) Q.-X. Zhou, Y. Guo, Y.-F. Zhu, *Nat. Catal.* **2023**, *6*, 574–584; i) Y. Guo, Q.-X. Zhou, J. Nan, W.-X. Shi, F.-Y. Cui, Y.-F. Zhu, *Nat. Commun.* **2022**, *13*, 2067; j) T. Li, B.-T. Liu, Z.-B. Fang, Q. Yin, R. Wang, T.-F. Liu, *J. Mater. Chem. A.* **2021**, *9*, 4687–4691; k) Y.-Q. Tang, M. Yuan, B.-J. Jiang, Y.-T. Xiao, Y. Fu, S. Chen, Z.-P. Deng, Q.-J. Pan, C.-G. Tian, H.-G. Fu, *J. Mater. Chem. A.* **2017**, *5*, 21979–21985.

[5] a) X.-Z. Luo, X.-J. Jia, J.-H. Deng, J.-L. Zhong, H.-J. Liu, K.-J. Wang, D.-C. Zhong, *J. Am. Chem. Soc.* **2013**, *135*, 11684–11687; b) Z.-J. Zhang, Y.-X. Ye, S.-C. Xiang, B.-L. Chen, *Acc. Chem. Res.* **2022**, *55*, 3752–3766; c) B. Wang, R.-B. Lin, Z.-J. Zhang, S.-C. Xiang, B.-L. Chen, *J. Am. Chem. Soc.* **2020**, *142*, 14399–14416; d) H.-L. Zheng, J.-Q. Zhao, Y.-Y. Sun, A.-A. Zhang, Y.-J. Cheng, L. He, X.-H. Bu, J. Zhang, Q.-P. Lin, *J. Am. Chem. Soc.* **2023**, *145*, 27728–27739.

[6] a) S.-S. Hu, C.-F. Xie, Y.-P. Xu, X.-L. Chen, M.-L. Gao, H. Wang, W.-J. Yang, Z.-N. Xu, G.-C. Guo, H.-L. Jiang, *Angew. Chem. Int. Ed.* **2023**, *62*, e202311625; *Angew. Chem.* **2023**, *135*, e202311625; b) Y. Li, J.-F. Sui, L.-S. Cui, H.-L. Jiang, *J. Am. Chem. Soc.* **2023**, *145*, 1359–1366; c) Y.-H. Wang, Y.-X. Ren, Y. Cao, X. Liang, G.-W. He, H.-Z. Ma, H.-L. Dong, X. Fang, F.-S. Pan, Z.-Y. Jiang, *Nano-Micro Lett.* **2023**, *15*, 50.

[7] a) G.-X. Lan, Y.-J. Fan, W.-J. Shi, E. You, S. S. Veroneau, W.-B. Lin, *Nat. Catal.* **2022**, *5*, 1006–1018; b) S. Suleman, Y. Zhang, Y.-Y. Qian, J.-W. Zhang, Z.-Y. Lin, O. Metin, Z. Meng, H.-L. Jiang, *Angew. Chem. Int. Ed.* **2024**, *63*, e202314988; *Angew. Chem.* **2024**, *136*, e202314988.

[8] a) S.-Y. Wang, Z.-W. Ai, X.-W. Niu, W.-J. Yang, R. Kang, Z.-Y. Lin, A. Waseem, L. Jiao, H.-L. Jiang, *Adv. Mater.* **2023**, *35*, e2302512; b) W.-B. Chen, L. Wang, D.-Z. Mo, F. He, Z.-L. Wen, X.-J. Wu, H.-X. Xu, L. Chen, *Angew. Chem. Int. Ed.* **2020**, *59*, 16902–16909; *Angew. Chem.* **2020**, *132*, 17050–17057; c) T. Wang, M.-J. Li, Y.-J. Chen, X.-P. Che, F.-Z. Bi, Y. Yang, R.-Q. Yang, C.-X. Li, *ACS Catal.* **2023**, *13*, 15439–15447; d) Y. Mou, X.-D. Wu, C.-C. Qin, J.-Y. Chen, Y.-L. Zhao, L.-B. Jiang, C. Zhang, X.-Z. Yuan, E. Huixiang Ang, H. Wang, *Angew. Chem. Int. Ed.* **2023**, *62*, e202309480; *Angew. Chem.* **2023**, *135*, e202309480; e) J. Cheng, Y.-T. Wu, W. Zhang, J. Zhang, L. Wang, M. Zhou, F.-T. Fan, X.-J. Wu, H.-X. Xu, *Adv. Mater.* **2023**, *35*, e2305313.

[9] M. Marmier, G. Cecot, B. F. E. Curchod, P. Pattison, E. Solari, R. Scopellitia, K. Severin, *Dalton Trans.* **2016**, *45*, 8422–8427.

[10] a) X. Song, Y. Wang, C. Wang, D. Wang, G. Zhuang, K. O. Kirlikovali, P. Li, O. K. Farha, *J. Am. Chem. Soc.* **2022**, *144*, 10663–10687; b) N. Liu, J. Jiang, Z. Chen, B. Wu, S. Zhang, Y.-Q. Zhang, P. Cheng, W. Shi, *Angew. Chem. Int. Ed.* **2023**, *62*, e202312306; *Angew. Chem.* **2023**, *135*, e202312306; c) L. Gong, Y. Ye, Y. Liu, Y. Li, Z. Bao, S. Xiang, Z. Zhang, B. Chen, *ACS Appl. Mater. Interfaces* **2022**, *14*, 19623–19628.

[11] a) M.-C. Guo, Q.-Q. Meng, W.-Y. Chen, Z. Meng, M.-L. Gao, Q.-X. Li, X.-Z. Duan, H.-L. Jiang, *Angew. Chem. Int. Ed.* **2023**, *62*, e202305212; *Angew. Chem.* **2023**, *135*, e202305212; b) B. Ma, M. Blanco, L. Calvillo, L.-J. Chen, G. Chen, T. C. Lau, G. Drazic, J. Bonin, M. Robert, G. Granozzi, *J. Am. Chem. Soc.* **2021**, *143*, 8414–8425; c) J.-H. Zhang, Y.-N. Gong, H.-J. Wang, Y.-C. Wang, W. Yang, J.-H. Mei, D.-C. Zhong, T.-B. Lu, *Proc. Natl. Acad. Sci. USA* **2022**, *119*, e2118278119.

[12] a) J.-Q. Liu, J.-F. Miao, S. Ullah, K. Zhou, L. Yu, H. Wang, Y.-F. Wang, T. Thonhauser, J. Li, *ACS Materials Lett.* **2022**, *4*,

1227–1232; b) P. Y. You, K.-M. Mo, Y.-M. Wang, Q. Gao, X.-C. Lin, J.-T. Lin, M. Xie, R.-J. Wei, G.-H. Ning, D. Li, *Nat. Commun.* **2024**, *15*, 194; c) Q. Li, J.-N. Chang, Z.-M. Wang, M. Lu, C. Guo, M. Zhang, T.-Y. Yu, Y.-F. Chen, S.-L. Li, Y.-Q. Lan, *J. Am. Chem. Soc.* **2023**, *145*, 23167–23175.

[13] a) Y.-N. Gong, J.-H. Mei, W.-J. Shi, J.-W. Liu, D.-C. Zhong, T.-B. Lu, *Angew. Chem. Int. Ed.* **2024**, *63*, e202318735; b) T.-Y. Zheng, X. Ding, T.-T. Sun, X.-Y. Yang, X.-X. Wang, X. Zhou, P.-P. Zhang, B.-Q. Yu, Y.-H. Wang, Q.-M. Xu, L.-B. Xu, D.-S. Wang, J.-Z. Jiang, *Small.* **2023**, e2307743; c) F.-M. Zhang, J.-L. Sheng, Z.-D. Yang, X.-J. Sun, H.-L. Tang, M. Lu, H. Dong, F.-C. Shen, J. Liu, Y.-Q. Lan, *Angew. Chem. Int. Ed.* **2018**, *57*, 12106–12110; *Angew. Chem.* **2018**, *130*, 12282–12286.

[14] a) Y.-Y. Qian, Y.-L. Han, X.-Y. Zhang, G. Yang, G.-Z. Zhang, H.-L. Jiang, *Nat. Commun.* **2023**, *14*, 3083; b) Y. Bai, L. Wilbraham, B. J. Slater, M. A. Zwijnenburg, R. S. Sprick, A. I. Cooper, *J. Am. Chem. Soc.* **2019**, *141*, 9063–9071; c) Y.-Y. Wan, L. Wang, H.-X. Xu, X.-J. Wu, J.-L. Yang, *J. Am. Chem. Soc.* **2020**, *142*, 4508–4516.

[15] a) B. Wang, R. He, L.-H. Xie, Z.-J. Lin, X. Zhang, J. Wang, H.-L. Huang, Z.-J. Zhang, K. S. Schanze, J. Zhang, S.-C. Xiang, B.-L. Chen, *J. Am. Chem. Soc.* **2020**, *142*, 12478–12485; b) Z.-A. Lan, G.-G. Zhang, X. Chen, Y.-F. Zhang, K. A. I. Zhang, X.-C. Wang, *Angew. Chem. Int. Ed.* **2019**, *58*, 10236–10240; *Angew. Chem.* **2019**, *131*, 10342–10346; c) J. Bian, Z. Zhang, J. Feng, M. Thangamuthu, F. Yang, L. Sun, Z. Li, Y. Qu, D. Tang, Z. Lin, F. Bai, J. Tang, L. Jing, *Angew. Chem. Int. Ed.* **2021**, *60*, 20906–20914; *Angew. Chem.* **2021**, *133*, 21074–21082.

[16] Y.-N. Gong, W.-H. Zhong, Y. Li, Y.-Z. Qiu, L.-R. Zheng, J. Jiang, H.-L. Jiang, *J. Am. Chem. Soc.* **2020**, *142*, 16723–16731.

[17] a) J.-X. Low, B.-Z. Dai, T. Tong, C.-J. Jiang, J.-G. Yu, *Adv. Mater.* **2019**, *31*, 1802981; b) Z.-C. Kong, J.-F. Liao, Y.-J. Dong, Y.-F. Xu, H.-Y. Chen, D.-B. Kuang, C.-Y. Su, *ACS Energy Lett.* **2018**, *3*, 2656–2662.

[18] a) T. Banerjee, F. Haase, G. Savasci, K. Gottschling, C. Ochsenfeld, B. V. Lotsch, *J. Am. Chem. Soc.* **2017**, *139*, 16228–16234; b) P. Wang, G. Liang, M. R. Reddy, M. Long, K. Driskill, C. Lyons, B. Donnadieu, J. C. Bollinger, C. E. Webster, X. Zhao, *J. Am. Chem. Soc.* **2018**, *140*, 9219–9229; c) Y. Zheng, J. Dong, C. Huang, L. Xia, Q. Wu, Q. Xu, W. Yao, *Appl. Catal. B* **2020**, *260*, 118220; d) Z. Li, J.-D. Xiao, H.-L. Jiang, *ACS Catal.* **2016**, *6*, 5359–5365.

Manuscript received: March 20, 2024
Accepted manuscript online: June 21, 2024
Version of record online: ■■, ■■

Research Article

HOFs

C.-J. Lu, W.-J. Shi, Y.-N. Gong,* J.-H. Zhang, Y.-C. Wang, J.-H. Mei, Z.-M. Ge, T.-B. Lu, D.-C. Zhong* **e202405451**

Modulating the Microenvironments of Robust Metal Hydrogen-Bonded Organic Frameworks for Boosting Photocatalytic Hydrogen Evolution

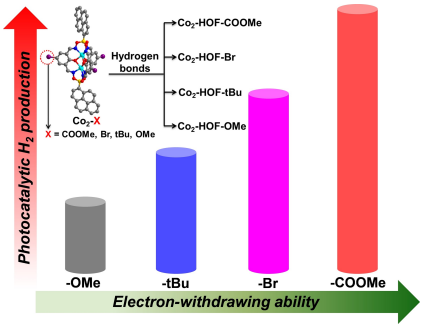

Four robust metal hydrogen-bonded organic frameworks with different electron-withdrawing ability of functional groups have been successfully constructed, which exhibit distinctly different photocatalytic activity for hydrogen evolution, for the first time, highlighting the microenvironment modulation in HOFs plays an important role in regulating photocatalysis.